RSC Advances

PAPER

View Article Online
View Journal | View Issue

Cite this: *RSC Adv.*, 2017, **7**, 36688

On the corrosion inhibition of carbon steel in 1 M HCl with a pyridinium-ionic liquid: chemical, thermodynamic, kinetic and electrochemical studies

Sami Ben Aoun *

The efficiency of 1-hexylpyridinium bromide (NR3) ionic liquid for the corrosion inhibition of carbon steel in 1 M hydrochloric acid has been investigated by gravimetric, linear polarization (LPR), electrochemical impedance spectroscopy (EIS) and scanning electron microscopy (SEM) techniques. Increasing NR3 concentration led to increasing inhibition efficiency (IE%) following the increasing surface coverage (θ). Thermodynamic studies revealed a decreasing IE% with increasing temperature proven to be due to the physical nature of the adsorption mechanism of NR3 which was shown to obey a Langmuir isotherm. LPR elucidated the mixed type inhibition effect of NR3 and its effective blocking of both cathodic and anodic corrosion sites on the carbon steel surface leading to decreased current densities of both Tafel branches without altering the corrosion mechanism. EIS results confirmed the adsorptive behavior of the investigated ionic liquid in replacement of the initially adsorbed water molecules and the formation of a protective film leading to increasing charge-transfer resistance as a result of decreasing double layer capacitance with increasing concentrations. The IE% attained *ca.* 88.6% in the presence of as low as 3×10^{-3} M NR3 inferring the high inhibitory effect of the studied compound. SEM micrographs confirmed the formation and growth of a protective layer reaching a dense coverage at the optimum concentration.

Received 10th April 2017
Accepted 20th July 2017

DOI: 10.1039/c7ra04084a

rsc.li/rsc-advances

1. Introduction

Mineral acids are widely used, among others, in oil well acidizing, acid pickling and acid descaling.[1–4] This results in the chemical attack of less noble metals, for instance steel, which leads to its corrosion occurring generally *via* electrochemical anodic dissolution[5] and causes several economical and safety problems.[6–8] The use of corrosion inhibitors, mainly organic compounds, was revealed to be one of the most effective methods for corrosion control and, hopefully, its prevention.[9–16] Higher inhibition efficiencies are generally achieved with compounds comprising in their molecular structures P, O, S, N, π-electrons and aromatic rings.[17–31] The inhibitive activity of such compounds lies in their ability to reduce the corrosion rates *via* strong adsorption on the corroding metal surface.[21,32–34] Nevertheless, health hazards and environmental issues are the major drawbacks of several corrosion inhibitors which justify the tremendous efforts deployed to substitute them with more eco-friendly compounds.[31,35] In this respect, ionic liquids emerged in recent decade as a new class of green corrosion inhibitors.[30,32,33,36–42]

The present paper investigates the inhibitory effect of 1-hexylpyridinium bromide (NR3) ionic liquid on the carbon steel corrosions in aggressive hydrochloric acid solution using both chemical (*i.e.* gravimetric) and electrochemical (linear polarization and electrochemical impedance spectroscopy) techniques. Complementarity and correlations of these techniques will be highlighted and details about the thermodynamics and kinetics of the inhibition process will be elucidated. The morphology of the corroding metal will be monitored, both in the absence and presence of inhibitor, with the aid of scanning electron microscopy.

2. Experimental

2.1. Chemicals and materials

The structure of the investigated ionic liquid is shown in Scheme 1. For convenience, this compound will be denoted as (NR3) in the rest of the text. Acetone (99.5%) and hydrochloric acid (37%) were purchased from Panreac along with ethanol (99.8%, Sigma-Aldrich) and were used as described subsequently. All solutions were prepared in distilled water. 0.5 mm thick carbon-steel sheets were cut into various sizes in order to prepare the specimens for subsequent experiments.

Department of Chemistry, Faculty of Science, Taibah University, PO. Box 30002, Al Madinah Al Munawarah, Kingdom of Saudi Arabia. E-mail: sbenaoun@taibahu.edu.sa; Fax: +966 148618888 ext. 4326; Tel: +966 590900727

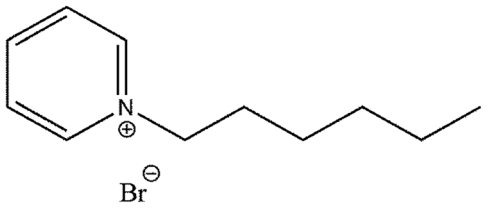

Scheme 1 Chemical structure of 1-hexylpyridinium bromide (NR3).

2.2. Weight loss measurements

Precisely weighted carbon steel samples (GR-202 analytical balance, A&D Co., Ltd., Japan) were first mechanically polished then cleaned with copious amounts of distilled water, acetone and ethanol. The as-prepared specimen was then immersed for 5 hours in corrosive media (15 cm^2 exposed surface area) either in the absence or presence of various inhibitor concentrations (*i.e.* 10^{-5} to 3×10^{-3} M). In all experiments, the corrosive media volume was kept constant (*i.e.* 50 mL).

Unless otherwise specified, the working temperature was *ca.* 294 ± 1 K.

2.3. Thermodynamics study

The temperature effect was investigated in the temperature range 294–343 K and the thermostatic conditions were ensured by means of a digitally-controlled water bath (Yudian Automation Technology, Hong Kong, Co., Ltd.).

2.4. Electrochemical measurements

A conventional four-electrode corrosion cell (500 mL), comprising two platinum sheets counter electrodes, a saturated calomel reference electrode (SCE) jacked in a Luggin capillary and the as-prepared carbon steel specimen working electrode (1 cm^2 cut), was employed in all electrochemical measurements. The experiments were carried out using an Autolab PGSTAT 128N instrument equipped with an FRA32M frequency response analyzer module (Metrohm Autolab B.V, The Netherlands). Data acquisition and analysis were done with NOVA 2.1 software.

In linear polarization (LPR) experiments, a 1 mV step potential was imposed while the potential was scanned *vs.* corrosion potential (E_{corr}) in the interval −100 mV to 100 mV at 1 mV s^{-1} scan rate. While for the electrochemical impedance spectroscopy (EIS) measurements, a perturbation wave of single sine and an amplitude of 10 mV was applied with a 0.125 s integration time and the frequency was scanned in the range 100 kHz to 50 mHz at the open circuit potential (OCP).

Prior to each experiment, a 30 min pre-conditioning of the working electrode was enough to reach a steady value of OCP.

2.5. Surface characterization

The morphology of the corroding carbon steel surface before and after corrosion tests either in the presence or absence of NR3 was characterized by scanning electron microscopy (SEM) with a JCM-6000 instrument (JEOL, Japan) operating under high vacuum and with 15 kV acceleration voltage.

3. Results and discussion

3.1. Gravimetric study

The results of corrosion tests in 1 M HCl at 294 K for the corrosion of carbon steel in presence of various concentrations of (NR3) are displayed in Table 1. The following equations[33] were used to calculate the corrosion rate (CR), the inhibition efficiencies (IE%) and the surface coverage (θ) of Table 1:

$$CR = \frac{\Delta W}{At} \quad (1)$$

$$IE\% = \left[\frac{CR^0 - CR^i}{CR^0}\right] \times 100 \quad (2)$$

$$\theta = \frac{IE\%}{100} \quad (3)$$

where ΔW (mg) is the weight loss, A (cm^2) the exposed surface area, t (h) the exposure time, IE% is the inhibition efficiency, CR^0 and CR^i are respectively, the corrosion rate in the absence and presence of inhibitor and θ the surface coverage.

As clearly shown, the corrosion rate decreases with increasing concentrations of NR3 leading to a pronounced inhibition efficiency increase and that is graphically presented in Fig. 1, reaching 82.4% with the addition of just 3 mM NR3 to the aggressively corrosive molar hydrochloric acid. Such behavior is indicative of the high inhibitive activity of the investigated ionic liquid which might be explained by the diminishing of the exposed metal surface to corrosive solution as a consequence of increasing number of adsorbed NR3 molecules in replacement of water molecules leading to a higher surface coverage,[33] shown here as an increase of θ values (*cf.* Table 1) and hindering the metal dissolution process.[43–45]

Table 1 Results of the kinetic study in 1 M HCl at 294 K for the corrosion of carbon steel in presence of various concentrations of (NR3)

[NR3] (mol L^{-1})	0	10^{-5}	10^{-4}	10^{-3}	3×10^{-3}
CR (mg cm^{-2} h^{-1})	$(205 \pm 4) \times 10^{-3}$	$(145 \pm 6) \times 10^{-3}$	$(99 \pm 1) \times 10^{-3}$	$(53 \pm 5) \times 10^{-3}$	$(36 \pm 3) \times 10^{-3}$
IE%	—	29.4 ± 3.2	51.5 ± 1.0	74.0 ± 2.6	82.4 ± 1.3
θ	—	$(294 \pm 32) \times 10^{-3}$	$(515 \pm 10) \times 10^{-3}$	$(740 \pm 26) \times 10^{-3}$	$(824 \pm 13) \times 10^{-3}$
log[NR3]	—	−5.00	−4.00	−3.00	−2.52
log CR	−0.688	−0.840	−1.003	−1.273	−1.444
n			−0.243		
k (mg cm^{-2} h^{-1})$^{1/n}$			9.528×10^{-3}		

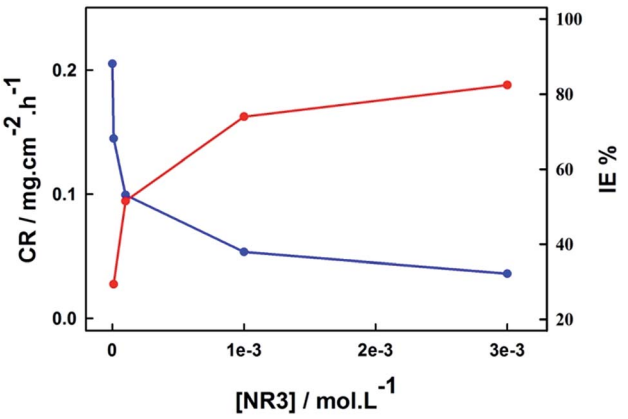

Fig. 1 Effect of NR3 concentration on carbon steel corrosion rate (blue) and inhibition efficiency (red) in 1 M HCl at 294 K.

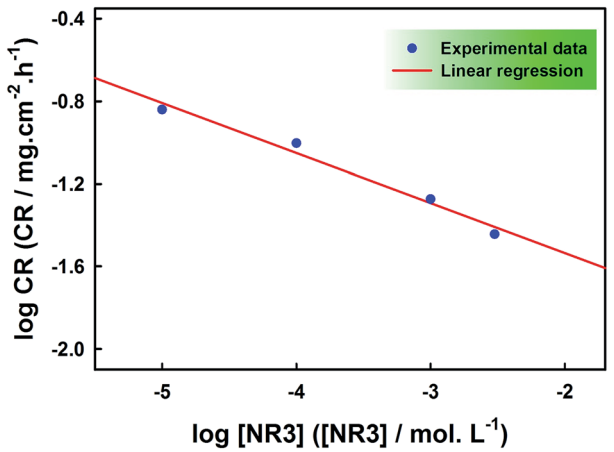

Fig. 2 log CR *vs.* log[NR3] plot for the corrosion of carbon steel in 1 M HCl at 294 K.

3.2. Thermodynamics and kinetics

The kinetics of carbon steel corrosion in the presence of various concentrations of NR3 compound can be examined based on the following equation:[46]

$$\mathrm{CR} = k[\mathrm{NR3}]^n \quad (4)$$

n reflects the order of the corrosion reaction and k being the specific rate constant in the present work conditions. For a first order kinetics, the units of k will be same as the corrosion rate (*i.e.* mg cm^{-2} h^{-1}). The graphical presentation of eqn (4) is the linear plot of log CR *vs.* log[NR3] as displayed in Fig. 2.

The good linearity of Fig. 2 ($R^2 = 0.978$) is a proof that the corrosion rate in the current study obeys eqn (4) and the values of constants n and k can be respectively calculated from the slope and the y-intercept and the values are included with the experimental data points given in Table 1.

The inverse proportionality of the corrosion rate and NR3 concentration is revealed by the negative sign of (n) and its value infers the good inhibition efficiency of the investigated ionic liquid.[32,33]

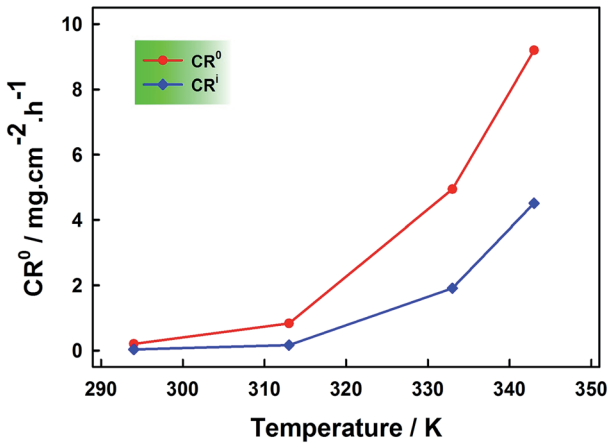

Fig. 3 Temperature effect on the carbon steel corrosion rate in presence (CR^i) and the absence (CR^0) of 3×10^{-3} M NR3 in 1 M HCl.

Furthermore, the temperature effect on corrosion rate was studied in the temperature range (294–343 K) both in the absence and presence of optimum NR3 concentration (*i.e.* 3×10^{-3} M) and results are displayed in Fig. 3 and the extracted data is summarized in the following Table 2.

As expected, both cases exhibited an increasing corrosion rate with increasing temperature and in the whole temperature range investigated the corrosion proceeds at higher rates in the absence of inhibitor compound as revealed in Fig. 3. Nevertheless, the increase in the corrosion rate was more pronounced (*i.e.* 125 folds) in the case of inhibited corrosion compared to uninhibited cases (*i.e.* 45 folds) inferring an inhibition efficiency decrease with increasing temperature as shown in Fig. 4. This trend is most likely a consequence of the physical adsorption (physisorption) onto the corroding metal surface of the inhibitor (NR3) molecules[32] that weakens at elevated temperatures[47] which, as consequence, decreases the number of the adsorbed inhibitor's molecules and eventually leads to their partial desorption.[48,49]

This can be further elucidated by calculating the activation energy (E_a) on the assumption that the corrosion rate-temperature dependence obeys the Arrhenius equation:[50]

$$\mathrm{CR} = A \exp\left[-\frac{E_a}{RT}\right] \quad (5)$$

The pre-exponential factor A having the same units of the corrosion rate, R is the universal gas constant, T is the absolute temperature and E_a the activation energy.

A plot of the corrosion rate natural logarithm against the absolute temperature reciprocal is shown in Fig. 5 and its good linearity both in the absence and presence of NR3 ($R^2 = 0.996$ and 0.987, respectively) confirms the Arrhenius-type dependence of the corrosion rate on temperature in the present work conditions.

The values of the pre-exponential factor and the activation energy extracted respectively, from the slopes and the y-intercepts of the best-fitting regression lines in Fig. 5 are given in

Table 2 Results of the gravimetric study in 1 M HCl at different temperatures for the corrosion of carbon steel in presence of 3×10^{-3} M (NR3)

T (K)	CR^0 (mg cm^{-2} h^{-1})	CR^i (mg cm^{-2} h^{-1})	IE%	θ
294	$(205 \pm 4) \times 10^{-3}$	$(36 \pm 3) \times 10^{-3}$	82.4 ± 1.3	$(824 \pm 13) \times 10^{-3}$
313	$(835 \pm 36) \times 10^{-3}$	$(169 \pm 10) \times 10^{-3}$	79.8 ± 1.5	$(798 \pm 15) \times 10^{-3}$
333	$(4946 \pm 38) \times 10^{-3}$	$(1912 \pm 72) \times 10^{-3}$	61.3 ± 1.5	$(613 \pm 15) \times 10^{-3}$
343	$(9194 \pm 25) \times 10^{-3}$	$(4515 \pm 275) \times 10^{-3}$	50.9 ± 3.0	$(509 \pm 30) \times 10^{-3}$

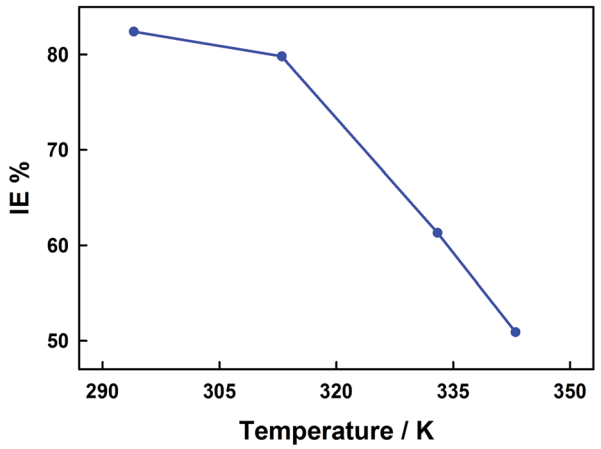

Fig. 4 Temperature effect on the carbon steel corrosion inhibition efficiency in the presence of 3×10^{-3} M NR3 in 1 M HCl.

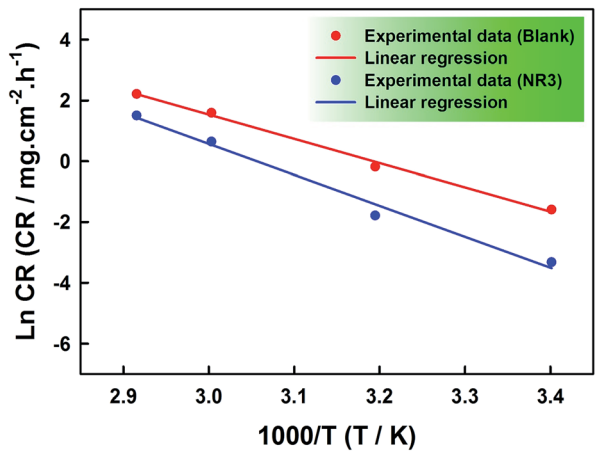

Fig. 5 ln CR *vs.* (1/*T*) plots for the corrosion of carbon steel in the absence and presence of 3×10^{-3} M NR3 in 1 M HCl.

Table 3. A clearly observable activation energy increase in the presence of the optimum concentration of NR3 (*i.e.* 3×10^{-3} M) shows the energy barrier increase of the corrosion process[48,50] and proves the NR3 molecules strong adsorption onto the carbon steel surface and by consequence the thickening of interfacial double layer[49] resulting in its high inhibitory activity towards the carbon steel corrosion in the present work conditions. Moreover, this increase favors the physical nature of NR3 adsorption onto the metal surface.[32,51]

The Arrhenius transition-state equation[32,33] applied to the investigated corrosion process allows the calculation of additional thermodynamic parameters:

$$CR = \frac{RT}{Nh} \exp\left(\frac{\Delta S_a}{R}\right) \exp\left(-\frac{\Delta H_a}{RT}\right) \quad (6)$$

where h is the Planck's constant, N is the Avogadro's number, R is the universal gas constant and ΔS_a and ΔH_a are the activation entropy and enthalpy of the corrosion process, respectively.

Plots of ln(CR/T) against the absolute temperature reciprocal for both uninhibited and inhibited corrosions are displayed in Fig. 6 and the various extracted parameters are included in Table 3. And here again, an activation enthalpy increase is observed in the presence of NR3 which is attributable to the existence of the ionic liquid cations at the interface of the corroding metal and the corrosive electrolyte.[46] On the other hand, lower values of ΔH_a compared to E_a, both in the absence and presence of corrosion inhibitor, are due to the hydrogen evolution reaction.[32,33] Additionally, the difference ($E_a - \Delta H_a =$ *ca.* 2.64 kJ) is constant for both cases and almost equal to the average value ($RT =$ *ca.* 2.67 kJ) in the present work conditions, indicating a unimolecular corrosion process.[32,33,51]

With regards to the entropy of activation (ΔS_a), examination of Table 3 results shows the ordering of the corroding metal surface in the rate-determining step as a consequence of the activated complex formation (negative sign of ΔS_a) against a clearly pronounced disorder (positive sign of ΔS_a) in the presence of inhibitor. The latter is then proven to be involved in a dissociation-type activation process.[7,32,52] Furthermore, the observed increase of ΔS_a is suggestive of water molecules replacement during NR3 adsorption onto the metal surface[53] as discussed in the previous section.

3.3. Adsorption isotherm

Adsorption isotherm enables the elucidation of the investigated ionic liquid inhibition mechanism through understanding its adsorptive strength and behaviour.[7,48,49] The data is usually analyzed *via* common adsorption isotherms fitting, namely: Freundlich, Temkin, Flory–Huggins, Frumkin and Langmuir.[7,34,48,49] In this work, the experimental data was best fitted to the Langmuir isotherm ($R^2 = 0.999$) where the ratio of NR3 concentration and surface coverage (θ) is plotted against the concentration [NR3] (*cf.* Fig. 7) as per the equation:

$$\frac{C_{inh}}{\theta} = \frac{1}{K_{ads}} + C_{inh} \quad (7)$$

Table 3 Results of the thermodynamic study in 1 M HCl for the corrosion of carbon steel in the presence and absence of 3×10^{-3} M NR3

Solution	Fig. 5 slope	Fig. 5 intercept	Fig. 6 slope	Fig. 6. intercept	A (mg cm^{-2} h^{-1})	E_a (kJ mol^{-1})	ΔH_a (kJ mol^{-1})	ΔS_a (J mol^{-1})
Blank	−7.986	25.498	−7.669	18.738	1.185×10^{11}	66.396	63.760	−41.751
NR3	−10.194	31.157	−11.180	24.396	3.399×10^{13}	84.753	82.117	5.289

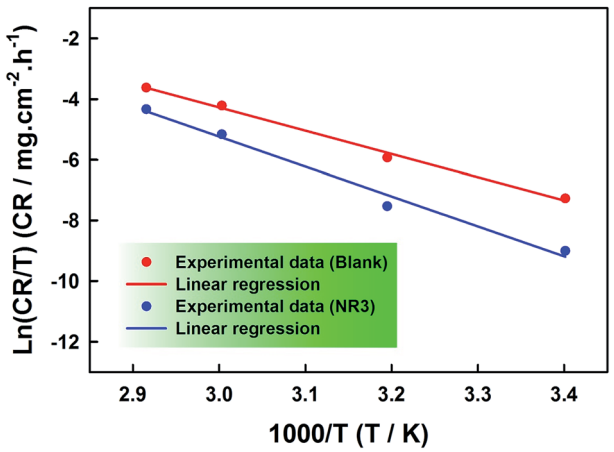

Fig. 6 ln(CR/T) *vs.* (1/T) plots for the corrosion of carbon steel in the absence and presence of 3×10^{-3} M NR3 in 1 M HCl.

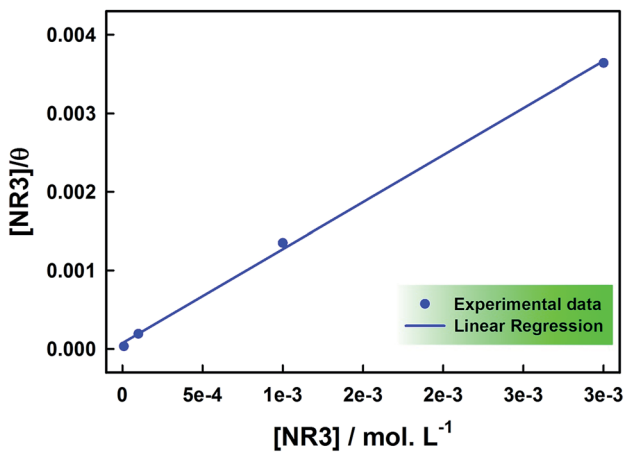

Fig. 7 Plot of [NR3]/θ *vs.* [NR3] for the corrosion of carbon steel in 1 M HCl at 294 K.

C_{inh}, θ and K_{ads} are the inhibitor molar concentration, the surface coverage and the adsorption constant, respectively.

The extracted data are given in Table 4. The regression line slope is found to be very close to unity and that confirms again that NR3 adsorption onto the carbon steel surface follows Langmuir adsorption. This is indicative that there is no intermolecular forces between the adsorbed ionic liquid's molecules.[50] The value of K_{ads} extracted from the y-intercept was used to calculate the adsorption free energy (ΔG_{ads}) using the equation:[34]

$$\Delta G_{ads} = -RT \ln(K_{ads} \times C_{solvent}) \quad (8)$$

where $C_{solvent} = 55.5$ mol L^{-1} for water.

The relatively large adsorption constant (*i.e. ca.* 13.353×10^3 mol^{-1} L) reveals the strong NR3 adsorption onto the corroding carbon steel surface[54] which explains the observed high inhibition efficiencies. Whereas, the negative sign of the adsorption free energy confirms that this adsorption process is indeed spontaneous. On the other hand, the value of (ΔG_{ads}) gives a clear indication about the nature of the adsorption process. In this respect, it is commonly agreed in literature that free energy values equal or less than 20 kJ mol^{-1} are indicative a physisorption process while those equal or higher than 40 kJ mol^{-1} reveal its chemisorption nature.[7,32–34,53,55,56] The value of ($\Delta G_{ads} = -33.037$ kJ mol^{-1}) obtained in the current work shows that a rather complex mixed-type adsorption is involved[32–34,49,53,57] and that is a predominantly physisorption.[32,58] This implies a predominant electrostatic interaction (physisorption) between NR3 and carbon steel in addition to electrons transfer or sharing (chemisorption) between NR3 molecules and the metal surface affecting most probably both anodic and cathodic sites.[32,44] Such behaviour would be expected based on NR3 structure (*cf.* Scheme 1), for instance the nitrogen lone pairs and π-bonds as well as the aromatic ring that would be the origin of this strong adsorption and inhibition effectiveness.[59,60] Further supporting results would be provided by electrochemical techniques.

Table 4 Adsorption parameters of NR3 in 1 M HCl onto the carbon steel surface

Inhibitor	Slope	K_{ads} (mol^{-1} L)	R^2	ΔG_{ads} (kJ mol^{-1})
NR3	1.196	13.353×10^3	0.999	−33.037

3.4. Linear polarization

Linear polarization (LPR) curves for carbon steel corrosion both in the presence and absence of different concentrations of NR3 in molar HCl solutions are reported in Fig. 8.

At a first sight, it is noteworthy that Tafel-type behavior is exhibited by both anodic and cathodic branches. In addition, all curves show similar shapes which proves that neither cathodic (*i.e.* hydrogen evolution reaction HER) nor anodic (*i.e.* metal dissolution) mechanisms were altered as a consequence of the inhibitor's addition into the corrosive solution.[53] From the Tafel lines extrapolation, we obtained various electrochemical parameters; cathodic slope (b_c), anodic slope (b_a), corrosion current (I_{corr}) and corrosion potential (E_{corr}) which are collected in Table 5.

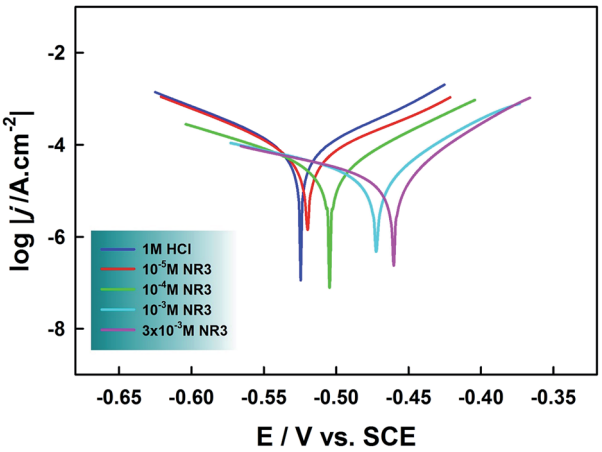

Fig. 8 Linear polarization of carbon steel in the presence of different concentrations of NR3 in 1 M HCl at 294 K.

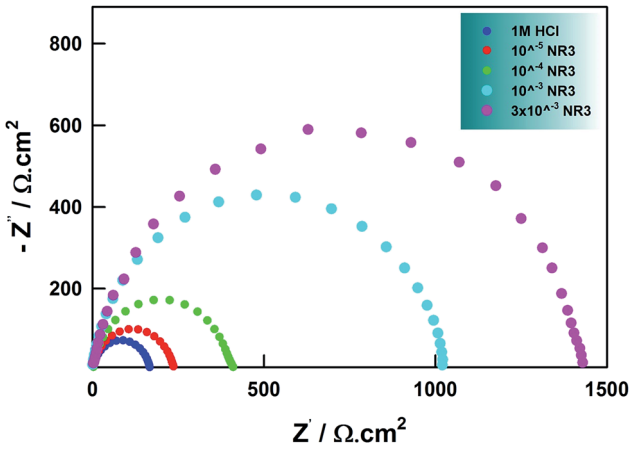

Fig. 9 Nyquist plots for carbon steel in the presence of different concentrations of NR3 in 1 M HCl at 294 K.

Inspection of Fig. 8 reveals parallel cathodic Tafel lines which indicate that HER is under activation (charge-transfer) control.[7,49,61] Also, there is no significant change in the values of both anodic and cathodic Tafel slopes upon addition of various concentrations of NR3 compound suggesting that the inhibition mechanism of the latter proceeds through blocking the active anodic and cathodic sites on the carbon steel surface.[62–64] The inhibitory effect of NR3 is also revealed as current densities decrease in both cathodic and anodic branches[50] though this effect is slightly more pronounced on the latter. The degree of diminishment in current densities is a key factor for the inhibition efficiency that is calculated from the equation:

$$\mathrm{IE}\% = \frac{I^0_{\mathrm{corr}} - I_{\mathrm{corr}}}{I^0_{\mathrm{corr}}} \times 100 \quad (9)$$

I_{corr} and I^0_{corr} are respectively, the corrosion current densities in the presence and absence of NR3.

Table 5 outlines steady inhibition efficiencies increase with increasing NR3 concentrations, reaching *ca.* 81.3% in the presence of $[\mathrm{NR3}] = 3 \times 10^{-3}$ M agreeing very well with the gravimetric study results. Such behavior would be explainable by an increased adsorption of NR3 molecules onto the metal/corrosive media interface[53] which is supported by the increasing surface coverage (*cf.* Table 5) which is calculated using the equation:[63]

$$\theta = 1 - \frac{I_{\mathrm{corr}}}{I^0_{\mathrm{corr}}} \quad (10)$$

Such increase results in the corrosion active sites blocking which leads to the effective corrosion protection of the metal surface.[7]

One more observation pertains to the corrosion potential which showed a slight positive shift increasing with increasing inhibitor concentration yet the maximum shift ($\Delta E_{\mathrm{corr}} = ca.$ 64 mV) remains below the threshold value 85 mV implying the mixed-type corrosion inhibitor classification of the investigated NR3 compound.[62]

3.5. Electrochemical impedance spectroscopy

Electrochemical impedance spectroscopy (EIS) has been extensively reported in literature as a non-destructive yet very powerful technique in corrosion studies enabling the elucidation of corrosion and inhibition mechanisms *via* providing useful information regarding the reaction kinetics and the surface properties through analysis of related impedance diagrams.[55]

EIS results for the present work are shown as Nyquist and Bode presentations in Fig. 9 and 10, respectively. The single semicircular capacitive loop in the absence of inhibitor (*cf.* Fig. 9) is an indication of a single charge transfer process controlling the carbon steel corrosion reaction in the present study conditions.[34] This shape was unaffected in the presence of NR3 at different concentrations revealing that the corrosion process activation-controlled nature was not changed, in agreement with (LPR) investigation.

The depressed semicircles in Nyquist plots and the slopes that differ from (−1) in Bode plots are due to surface

Table 5 Results of the LPR study in 1 M HCl at 294 K for the corrosion of carbon steel in presence of various concentrations of (NR3)

[NR3] (mol L^{-1})	E_{corr} (mV)	I_{corr} (A cm^{-2})	b_a (mV dec^{-1})	b_c (mV dec^{-1})	IE%	θ
Blank	−525	9.38×10^{-5}	86	86	—	—
10^{-5}	−520	7.11×10^{-5}	84	94	24.2	0.242
10^{-4}	−505	3.25×10^{-5}	68	105	65.3	0.653
10^{-3}	−472	2.01×10^{-5}	56	135	78.6	0.786
3×10^{-3}	−460	1.75×10^{-5}	55	129	81.3	0.813

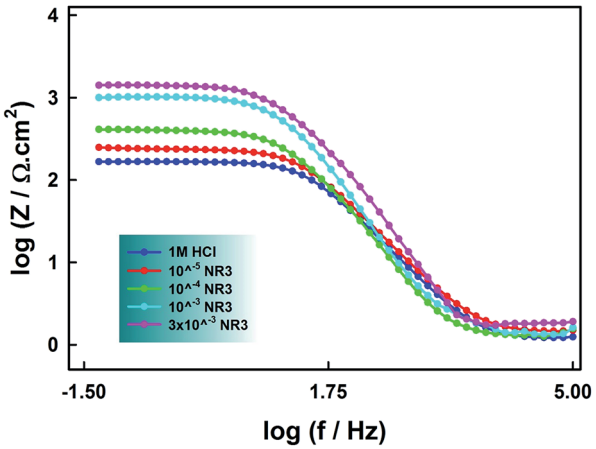

Fig. 10 Bode plots for carbon steel in the presence of different concentrations of NR3 in 1 M HCl at 294 K.

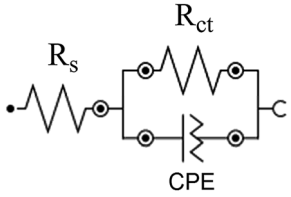

Scheme 2 Fitting equivalent circuit for the EIS data analysis.

irregularity-induced frequency dispersal of impedance at the metal-solution interface that is attributable to electrode surface inhomogeneity, usually its roughness.[48,50,63] Accordingly, instead of a regular capacitance, a constant-phase element (CPE) is included in the circuit model used for the EIS spectra analysis (*cf.* Scheme 2).

In that circuit, R_s and R_{ct} represent the solution and charge-transfer resistances, respectively. The latter is indirectly proportional to the corrosion rate and by monitoring its value change the inhibition efficiency can be calculated by the equation:

$$\mathrm{IE}\% = \frac{R_{ct}^0 - R_{ct}}{R_{ct}^0} \times 100 \quad (11)$$

R_{ct} and R_{ct}^0 represent the charge transfer resistances in the presence and absence of inhibitor, respectively.

The accurate double layer capacitance values were determined by introducing the CPE in the fitting equivalent circuit since the capacitive loops in Fig. 9 are not perfect semicircles as a consequence of surface irregularities and the impedance is given by the equation:[49]

$$Z_{\mathrm{CPE}} = \frac{1}{Y_0(jw)^n} \quad (12)$$

where $j = \sqrt{-1}$, w is the angular frequency, Y_0 and n are, respectively, the values of the CPE admittance and exponent. The latter is a measure of the surface inhomogeneity[34] ranging between $0.5 \leq n \leq 1$ for depressed semicircle capacitive loops[50] with the CPE acting as a perfect capacitance for $n = 1$.[63]

The double layer capacitance (C_{dl}) values are therefore determined using the expression:[34]

$$C_{dl} = \sqrt[n]{Y_0 R_{ct}^{1-n}} \quad (13)$$

All parameters are tabulated in Table 6.

A noteworthy feature in Fig. 10 is the increasing values of impedance with increasing NR3 concentration revealing the inhibitory effect of the investigated ionic liquid as a consequence of the corrosion process deceleration.[49] Inspection of Fig. 9 reveals a remarkable increase of the capacitive semicircles diameters with increasing NR3 concentration explained by an increase in the values of R_{ct} (*cf.* Table 6) suggesting a protective film formation onto the metal–electrolyte interface[53] which is also supported by a notable decrease of the C_{dl} values especially at higher concentration of NR3 revealing the inhibitor's molecules adsorption onto the corroding metal surface in replacement of initially-adsorbed water molecules.[55]

According to Helmholtz model, this trend of C_{dl} is attributable to either or both the increase of the protective film thickness (δ) or the decrease of the relative dielectric constant (ε_r) as per the equation:[55]

$$C_{dl} = \frac{\varepsilon_0 \times \varepsilon_r}{\delta} \quad (14)$$

These results corroborate well with those of weight loss and LPR investigations, proving again that the inhibition process of NR3 proceeds by adsorption onto the metal surface.

The observed C_{dl} decrease and R_{ct} increase results in increasing values of inhibition efficiencies reaching a value of ~*ca.* 90% for a concentration $[\mathrm{NR3}] = 3 \times 10^{-3}$ M with a similar trend of surface coverage (θ) by the adsorbed NR3 molecules, defined by the equation:

$$\theta = \frac{R_{ct}^0 - R_{ct}}{R_{ct}^0} \quad (15)$$

3.6. Scanning electron microscopy

Insight onto the morphology of the corroding carbon steel surface both in the presence and absence of NR3 compound at

Table 6 Results of the EIS study in 1 M HCl at 294 K for the corrosion of carbon steel in presence of various concentrations of (NR3)

[NR3] (mol L^{-1})	R_{ct}^0 (Ω cm^2)	R_{ct} (Ω cm^2)	IE%	θ	Y_0 (Mho cm^{-2})	n	C_{dl} (F cm^{-2})
Blank	166	166	—	—	5.28×10^{-5}	9.24×10^{-1}	3.57×10^{-5}
10^{-5}	166	236	29.7	0.297	4.74×10^{-5}	9.18×10^{-1}	3.17×10^{-5}
10^{-4}	166	406	59.1	0.591	5.23×10^{-5}	8.96×10^{-1}	3.34×10^{-5}
10^{-3}	166	1022	83.8	0.838	2.45×10^{-5}	9.00×10^{-1}	1.62×10^{-5}
3×10^{-3}	166	1452	88.6	0.886	2.10×10^{-5}	8.69×10^{-1}	1.24×10^{-5}

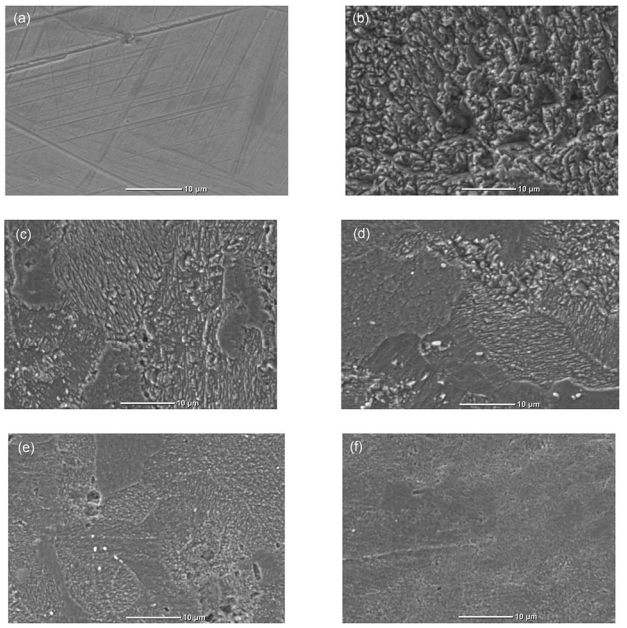

Fig. 11 SEM micrographs of (a) clean and (b–f) 1 M HCl-exposed carbon steel specimens for 5 hours at 294 K in the absence (b) and the presence of: (c) 10^{-5} M, (d) 10^{-4} M, (e) 10^{-3} M and (f) 3×10^{-3} M NR3.

various concentrations was achieved using scanning electron microscopy (SEM) and the respective micrographs are shown in Fig. 11.

It can be remarked that the high corrosion rate in molar HCl solution caused a clear damage of the metal surface (Fig. 11b) which is gradually avoided with increasing NR3 concentrations (Fig. 11c–f). The formation and growth of a protective film can be clearly noticed by successively comparing frames (c–f) of Fig. 11. It can be easily observed that the surface morphology of the corroding metal exposed to the aggressively corrosive media containing as less as 3 mM NR3 molecules reveals a dense, thick and nearly defect-free protective layer (*i.e.* Fig. 11a) providing an additional evidence of the highly efficient corrosion inhibition effect of the investigated compound.

4. Conclusion

In the present work, NR3 ionic liquid has shown efficient inhibition for the corrosion of carbon steel in 1 M HCl solution. In all used techniques, the increasing inhibitor concentration led to inhibition efficiency (IE%) increase. Very well-correlated results were obtained with small numerical difference in the values of (IE%) due to the exposure time difference between gravimetric and electrochemical investigations (*i.e.* 5 hours *vs.* 30 min). The temperature effect study revealed that the NR3 inhibition mechanism proceeds *via* adsorption onto the surface of the corroding metal following a Langmuir isotherm with a predominant physisorption nature and a decreasing IE% with increasing temperature. This was supported by the (LPR) results proving the mixed-type nature of the investigated inhibitor where it affects both cathodic and anodic reactions as speculated from the gravimetric results. Additionally, LPR investigations confirmed the adsorptive action of NR3 molecules through blocking the active anodic and cathodic sites on the carbon steel surface lowering both cathodic and anodic corrosion currents. That was further confirmed by EIS measurements that showed unchanged activation-controlled process either in presence or absence of NR3 inhibitor. Also, from the trend of R_{ct} and C_{dl} it was possible to confirm a protective film formation through the adsorption of NR3, replacing initially adsorbed water molecules. Monitoring of the surface morphology using SEM corroborated those findings by showing a steady growth of a protective film onto the corroding surface reaching a densely packed morphology at the optimum concentration (*i.e.* 3 mM) which showed the highest (IE%) in the present work conditions.

Acknowledgements

Prof. N. Raouafi is highly acknowledged for providing the NR3 compound.

References

1 D. Ben Hmamou, M. R. Aouad, R. Salghi, A. Zarrouk, M. Assouag, O. Benali, M. Messali, H. Zarrok and B. Hammouti, *J. Chem. Pharm. Res.*, 2012, **4**, 3489–3497.
2 A. H. Al Hamzi, H. Zarrok, A. Zarrouk, R. Salghi, B. Hammouti, S. S. Al-Deyab, M. Bouachrine, A. Amine and F. Guenoun, *Int. J. Electrochem. Sci.*, 2013, **8**, 2586–2605.
3 C. Crowe, J. Masmonteil and R. Thomas, *Oilfield Rev.*, 1992, **4**, 22.
4 R. Solmaz, *Corros. Sci.*, 2014, **81**, 75–84.
5 M. Messali, *J. Mater. Environ. Sci.*, 2011, **2**, 174–185.
6 V. S. Saji, *Recent Pat. Corros. Sci.*, 2010, **2**, 6–12.
7 M. R. Laamari, J. Benzakour, F. Berrekhis, A. Derja and D. Villemin, *Arabian J. Chem.*, 2016, **9**(suppl. 1), S245–S251.
8 S. Kharchouf, L. Majidi, M. Bouklah, B. Hammouti, A. Bouyanzer and A. Aouniti, *Arabian J. Chem.*, 2014, **7**, 680–686.
9 M. Yadav, D. Sharma and S. Kumar, *Korean J. Chem. Eng.*, 2015, **32**, 993–1000.
10 S. A. S. Dias, S. V. Lamaka, C. A. Nogueira, T. C. Diamantino and M. G. S. Ferreira, *Corros. Sci.*, 2012, **62**, 153–162.
11 M. Yu, M. Liang, J. Liu, S. Li, B. Xue and H. Zhao, *Appl. Surf. Sci.*, 2016, **363**, 229–239.
12 S. Peng, W. Zhao, H. Li, Z. Zeng, Q. Xue and X. Wu, *Appl. Surf. Sci.*, 2013, **276**, 284–290.
13 E. Roussi, A. Tsetsekou, A. Skarmoutsou, C. A. Charitidis and A. Karantonis, *Surf. Coat. Technol.*, 2013, **232**, 131–141.
14 I. Santana, A. Pepe, E. Jimenez-Pique, S. Pellice, I. Milošev and S. Ceré, *Surf. Coat. Technol.*, 2015, **265**, 106–116.
15 A. C. Balaskas, I. A. Kartsonakis, D. Snihirova, M. F. Montemor and G. Kordas, *Prog. Org. Coat.*, 2011, **72**, 653–662.
16 S. Zheng and J. Li, *J. Sol–Gel Sci. Technol.*, 2010, **54**, 174–187.
17 M. Dahmani, A. Et-Touhami, S. S. Al-Deyab, B. Hammouti and A. Bouyanzer, *Int. J. Electrochem. Sci.*, 2010, **5**, 1060–1069.

18 A. Y. Musa, A. A. H. Kadhum, A. B. Mohamad, M. S. Takriff, A. R. Daud and S. K. Kamarudin, *Corros. Sci.*, 2010, **52**, 526–533.
19 E. M. Sherif and S. M. Park, *J. Electrochem. Soc.*, 2005, **152**, B428–B433.
20 E. M. Sherif and S. M. Park, *Electrochim. Acta*, 2006, **51**, 1313–1321.
21 S. Ben Aoun, M. Bouklah, K. F. Khaled and B. Hammouti, *Int. J. Electrochem. Sci.*, 2016, **11**, 7343–7358.
22 K. R. Ansari, M. A. Quraishi and A. Singh, *Measurement*, 2015, **76**, 136–147.
23 M. Yadav, S. Kumar, U. Sharma and P. N. Yadav, *J. Mater. Environ. Sci.*, 2013, **4**, 691–700.
24 K. R. Ansari, Sudheer, A. Singh and M. A. Quraishi, *J. Dispersion Sci. Technol.*, 2015, **36**, 908–917.
25 N. Caliskan and E. Akbas, *Mater. Chem. Phys.*, 2011, **126**, 983–988.
26 X. Li, X. Xie, S. Deng and G. Du, *Corros. Sci.*, 2014, **87**, 27–39.
27 L. Bai, L.-J. Feng, H.-Y. Wang, Y.-B. Lu, X.-W. Lei and F.-L. Bai, *RSC Adv.*, 2015, **5**, 4716–4726.
28 A. O. Yüce and G. Kardaş, *Corros. Sci.*, 2012, **58**, 86–94.
29 M. A. Chidiebere, E. E. Oguzie, L. Liu, Y. Li and F. Wang, *Mater. Chem. Phys.*, 2015, **156**, 95–104.
30 M. Finšgar and D. Kek Merl, *Corros. Sci.*, 2014, **83**, 164–175.
31 S. Hari Kumar and S. Karthikeyan, *J. Mater. Environ. Sci.*, 2013, **4**, 675–684.
32 S. Ben Aoun, *Pharma Chem.*, 2013, **5**, 294–304.
33 S. Ben Aoun, *Int. J. Electrochem. Sci.*, 2013, **8**, 10788–10804.
34 H. Lgaz, R. Salghi, S. Jodeh and B. Hammouti, *J. Mol. Liq.*, 2017, **225**, 271–280.
35 B. Zhang, C. He, C. Wang, P. Sun, F. Li and Y. Lin, *Corros. Sci.*, 2015, **94**, 6–20.
36 X. Zhou, H. Yang and F. Wang, *Electrochim. Acta*, 2011, **56**, 4268–4275.
37 P. Huang, J.-A. Latham, D. R. MacFarlane, P. C. Howlett and M. Forsyth, *Electrochim. Acta*, 2013, **110**, 501–510.
38 N. V. Likhanova, M. A. Domínguez-Aguilar, O. Olivares-Xometl, N. Nava-Entzana, E. Arce and H. Dorantes, *Corros. Sci.*, 2010, **52**, 2088–2097.
39 I. Lozano, E. Mazario, C. O. Olivares-Xometl, N. V. Likhanova and P. Herrasti, *Mater. Chem. Phys.*, 2014, **147**, 191–197.
40 Q. Zhang and Y. Hua, *Mater. Chem. Phys.*, 2010, **119**, 57–64.
41 X. Zheng, S. Zhang, W. Li, M. Gong and L. Yin, *Corros. Sci.*, 2015, **95**, 168–179.
42 M. Scendo and J. Uznanska, *Int. J. Corros.*, 2011, 2011.
43 F. Bentiss, M. Traisnel and M. Lagrenee, *Corros. Sci.*, 2000, **42**, 127–146.
44 L. Larabi, O. Benali and Y. Harek, *Mater. Lett.*, 2007, **61**, 3287–3291.
45 L. Larabi, Y. Harek, O. Benali and S. Ghalem, *Prog. Org. Coat.*, 2005, **54**, 256–262.
46 E. A. Noor, *Corros. Sci.*, 2005, **47**, 33–55.
47 L. Afia, N. Rezki, M. R. Aouad, A. Zarrouk, H. Zarrok, R. Salghi, B. Hammouti, M. Messali and S. S. Al-Deyab, *Int. J. Electrochem. Sci.*, 2013, **8**, 4346–4360.
48 J. Haque, K. R. Ansari, V. Srivastava, M. A. Quraishi and I. B. Obot, *J. Ind. Eng. Chem.*, 2017, **49**, 176–188.
49 K. R. Ansari, M. A. Quraishi, A. Singh, S. Ramkumar and I. B. Obote, *RSC Adv.*, 2016, **6**, 24130–24141.
50 V. V. Torres, V. A. Rayol, M. Magalhães, G. M. Viana, L. C. S. Aguiar, S. P. Machado, H. Orofino and E. D'Elia, *Corros. Sci.*, 2014, **79**, 108–118.
51 E. A. Noor, *Int. J. Electrochem. Sci.*, 2007, **2**, 996–1017.
52 I. El Ouali, B. Hammouti, A. Aouniti, Y. Ramli, M. Azougagh, E. M. Essassi and M. Bouachrine, *J. Mater. Environ. Sci.*, 2010, **1**, 1–8.
53 M. R. laamari, J. Benzakour, F. Berrekhis, M. Bakasse and D. Villemin, *Arabian J. Chem.*, 2016, **9**(suppl. 2), S1218–S1224.
54 A. Ghazoui, N. Bencaht, S. S. Al-Deyab, A. Zarrouk, B. Hammouti, M. Ramdani and M. Guenbour, *Int. J. Electrochem. Sci.*, 2013, **8**, 2272–2292.
55 R. Laamari, J. Benzakour, F. Berrekhis, A. Abouelfida, A. Derja and D. Villemin, *Arabian J. Chem.*, 2011, **4**, 271–277.
56 A. Zarrouk, H. Zarrok, R. Salghi, B. Hammouti, F. Bentiss, R. Touir and M. Bouachrine, *J. Mater. Environ. Sci.*, 2013, **4**, 177–192.
57 I. Ahamad, R. Prasad and M. A. Quraishi, *Corros. Sci.*, 2010, **52**, 1472–1481.
58 A. Guendouz, N. Missoum, A. Chetouani, S. S. Al-Deyab, B. Ben Cheikhe, N. Boussalah, B. Hammouti, M. Taleb and A. Aouniti, *Int. J. Electrochem. Sci.*, 2013, **8**, 4305–4327.
59 C. Verma, M. A. Quraishi and A. Singh, *J. Mol. Liq.*, 2015, **212**, 804–812.
60 C. B. Verma, E. E. Ebenso, I. Bahadur, I. B. Obot and M. A. Quraishi, *J. Mol. Liq.*, 2015, **212**, 209–218.
61 S. Issaadi, T. Douadi, A. Zouaoui, S. Chafaa, M. A. Khan and G. Bouet, *Corros. Sci.*, 2011, **53**, 1484–1488.
62 L. Fragoza-Mar, O. Olivares-Xometl, M. A. Domínguez-Aguilar, E. A. Flores, P. Arellanes-Lozada and F. Jiménez-Cruz, *Corros. Sci.*, 2012, **61**, 171–184.
63 S. Martinez and M. Metikoš-Huković, *J. Appl. Electrochem.*, 2003, **33**, 1137–1142.
64 M. Parveen, M. Mobin and S. Zehra, *RSC Adv.*, 2016, **6**, 61235–61248.